Supplement for

The single-particle mixing state and cloud scavenging of black carbon at a high-altitude mountain site in southern China

Guohua Zhang [1], Qinhao Lin [1, 2], Long Peng [1, 2], Xinhui Bi [1,*], Duohong Chen [3], Mei Li [4, 5], Lei Li [4, 5], Fred J. Brechtel [6], Jianxin Chen [7], Weijun Yan [7], Xinming Wang [1], Ping'an Peng [1], Guoying Sheng [1], Zhen Zhou [3]

[1]State Key Laboratory of Organic Geochemistry and Guangdong Key Laboratory of Environmental Resources Utilization and Protection, Guangzhou Institute of Geochemistry, Chinese Academy of Sciences, Guangzhou 510640, PR China

[2] Graduate University of Chinese Academy of Sciences, Beijing 100039, PR China

[3] State Environmental Protection Key Laboratory of Regional Air Quality Monitoring, Guangdong Environmental Monitoring Center, Guangzhou 510308, PR China

[4] Institute of Mass Spectrometer and Atmospheric Environment, Jinan University, Guangzhou 510632, China

[5] Guangdong Provincial Engineering Research Center for on-line source apportionment system of air pollution, Guangzhou 510632, China

[6] Brechtel Manufacturing Inc., Hayward, 94544, California, USA

[7] Shaoguan Environmental Monitoring Center, Shaoguan 512026, PR China

Correspondence should be addressed to Xinhui Bi (bixh@gig.ac.cn)

SPAMS

Individual particles are introduced into SPAMS through a critical orifice. They are focused and accelerated to specific velocities, determined by two continuous diode Nd:YAG laser beams (532 nm), which are used to trigger a pulsed laser (266 nm) to desorp/ionize the particles. The produced positive and negative molecular fragments are recorded. In summary, a velocity, a detection moment, and an ion mass spectrum are recorded for each ionized particle, while there is no mass spectrum for not ionized particles. The velocity could be converted to d_{va} based on a calibration using polystyrene latex spheres (PSL, Duke Scientific Corp., Palo Alto) with predefined sizes.

Aethalometer data analysis

The absorption coefficient is defined by Beer–Lambert's law (Arnott et al., 2005). A variable attenuation (ATN), is defined to represent the filter attenuation through the sample spot on a filter (Arnott et al., 2005; Weingartner et al., 2003; Backman et al., 2016). Aerosol light absorption coefficient and BC mass concentration can be calculated directly based on the measured ATN. It is well known that the measured ATN may differ from the true aerosol absorption due to 'filter loading effect', a phenomenon which appears as a gradual decrease of instrumental response as the aerosol loading on the filter increases (Arnott et al., 2005). Therefore, two calibration factors are introduced to convert aethalometer attenuation measurements to "real" absorption coefficient (Weingartner et al., 2003).

The AE-31 used in the present study may suffer from the effects described above. Differently, the AE-33 has been improved by the incorporation of a filter loading correction part, based on a two parallel spot measurement of optical absorption. It could provide a real-time output of the "loading compensation" parameter to compensate for the "loading effect". The details of the principle of operation, data deduction, and error budget of the AE-33, the inherent uncertainties in its technique and the corrections are extensively available in the literature (Drinovec et al., 2015).

Therefore, we reported EBC concentration from the results of AE-33. The noise level of the AE-33 at the time-base of 1 minute is < 0.016 Mm^{-1} for the b_{abs}, corresponding to 1 ng m^{-3} for the mass concentration of BC. As noted in the manuscript and Fig. S10, the EBC measured by AE-31 is significantly correlated ($R^2 = 0.9$, $p < 0.001$) with that measured by AE-33. Therefore, EBC concentrations derived from AE-31 were not corrected for the calculation of $Mf_{scav,EBC}$.

As shown in Fig. S10, AE-31 might underestimate ~15% of EBC for cloud INT particles in the calculation of $Mf_{scav,EBC}$. It is also noted that a threshold of 8 μm might underestimate the mass concentration of cloud RES EBC, since the size of droplets might extend to as low as 3 μm. Unfortunately, the size distribution of cloud droplets was not available for our study. Therefore, we assumed that the largest underestimate of cloud RES particles is 30% to assess the uncertainties for $Mf_{scav,EBC}$ calculation. The mean $Mf_{scav,EBC}$ was 30-36% when they were taken into account. Overall, the uncertainties for the calculation of $Mf_{scav,EBC}$ is with 10%.

Table S1. Average mass concentrations, mass fractions relative to fine particles and scavenged fractions of BC from the literatures.

Site	site type	season (year)	ave (± std) ($\mu g\ m^{-3}$)	mass fraction	$Mf_{scav,EBC}$ (%)	References
Shenzhen, Southern China	urban	Summer (2011)	4.0 ± 3.1	~11%	-[a]	(Lan, et al., 2013)
Guangzhou, Southern China	urban	Summer (2008)	8.86	-	-	(Wu, et al., 2013)
Guangzhou, Southern China	urban	Fall(2010)	4.3	~4%[b]	-	(Zhang, et al., 2013)
Shenzhen, Southern China	urban	Fall(2009)	6.0 ± 6.3	-	-	(Huang, et al., 2012)
Guangzhou, Southern China	Rural	Summer (2008)	2.62	-	-	(Wu, et al., 2013)
Ba Guang village, southern China	Rural	Fall(2009)	2.6 ± 1.0	-	-	(Huang, et al., 2012)
Mt. Soledad (251 m m.s.l.)	marine	Summer (2012)	0.07	-	-	(Schroder, et al., 2015)
Yongxing Island, Southern China	marine	Summer (2008)	0.54	-	-	(Wu, et al., 2013)
A coastal Chilean hill, (Valparaíso), 450 m a.s.l.	low-altitude	Winter (2013)	0.34 - 0.95	-	13 - 50	(Hitzenberger et al., 2016)
Puy de Dome (France), 1465 m a.s.l.	mid-altitude	Winter-spring (2001)	-	-	33 - 74	(Sellegri et al., 2003)
Nova Scotia, Canada (Below 1 km)	mid-altitude	Summer (1993)	0.06 ± 0.01	-	2 - 32	(Chylek et al., 1996)

[a] not available.

Nova Scotia, Canada (1-3 km)	mid-high-altitude	Summer (1993)	0.22 ± 0.03	-	-	(Chylek et al., 1996)
Mt. Rax (1644 m a.s.l.)	high-altitude	Spring (1999)	0.43	-	-	(Hitzenberger et al., 2001)
Mt. Rax (1644 m a.s.l.)	high-altitude	Spring (2000)	0.72	-	54 ± 25	(Hitzenberger et al., 2001)
Alpine Jungfraujoch (Switzerland), 3850 m a.s.l.	high-altitude	Summer (2004)	0.06	-	61	(*Cozic et al.*, 2007)
Alpine Jungfraujoch (Switzerland), 3850 m a.s.l.	high-altitude	Winter (2004)	0.05	-	-	(*Cozic et al.*, 2007)

[b] mass fraction relative to PM_3.

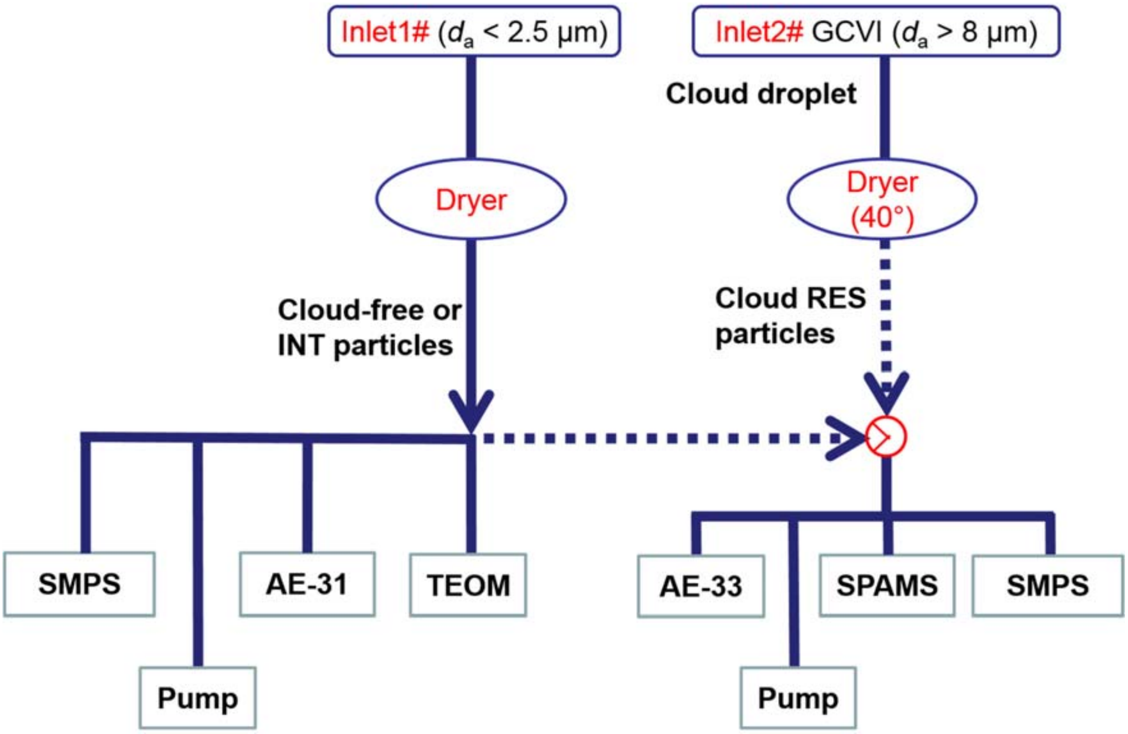

Figure S1. A scheme of the instrumentation setup in this study. The dash line illustrates that the sampling pipe was either connected to Inlet 1# or Inlet 2#. As described in section 2.1, the cloud INT and RES particles were intermittently measured by these instruments during Cloud III, through manually connect the sampling pipe to either Inlet 1# or Inlet 2# at approximately one-hour intervals.

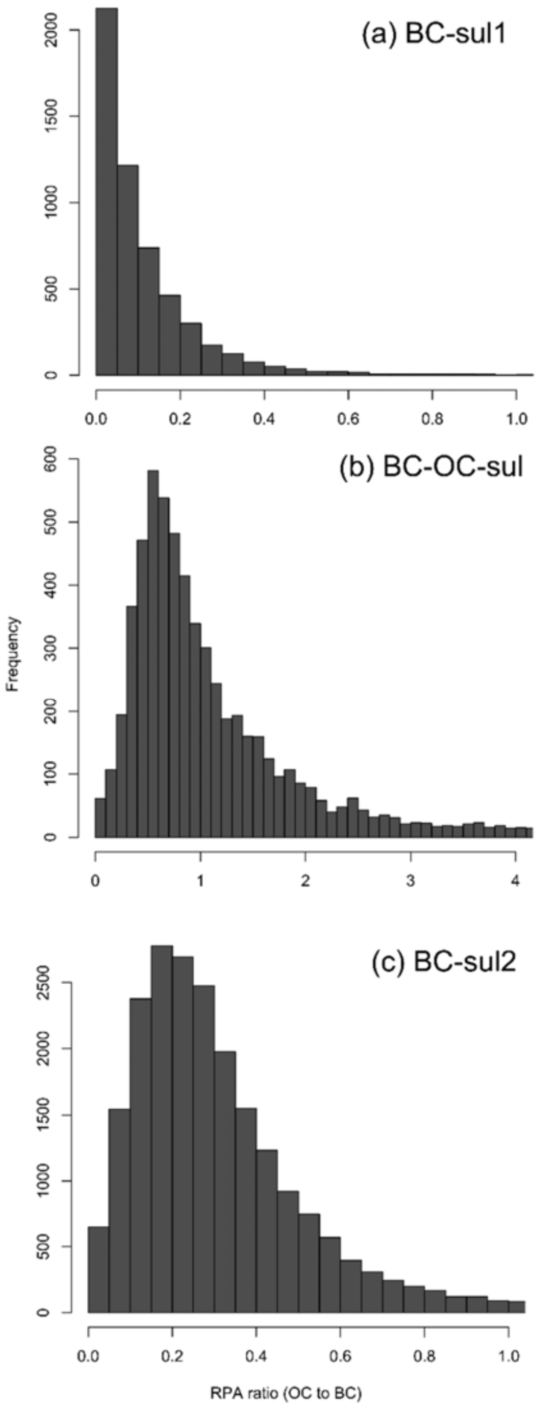
(a) BC-sul1
0
500
1000
1500
2000
0.0
0.2
0.4
0.6
0.8
1.0
(b) BC-OC-sul
Frequency
0
100
200
300
400
500
600
0
1
2
3
4
(c) BC-sul2
0
500
1000
1500
2000
2500
0.0
0.2
0.4
0.6
0.8
1.0
RPA ratio (OC to BC)

Figure S2. Statistic analysis on the RPA ratio of OC to BC in BC types. Markers were selected as m/z 27, 43, 50, 51, 61, 63, -26 for OC, and carbon ion clusters ($C_n^{+/-}$, $n \leq 5$) for BC, the same as those in Fig. 3.

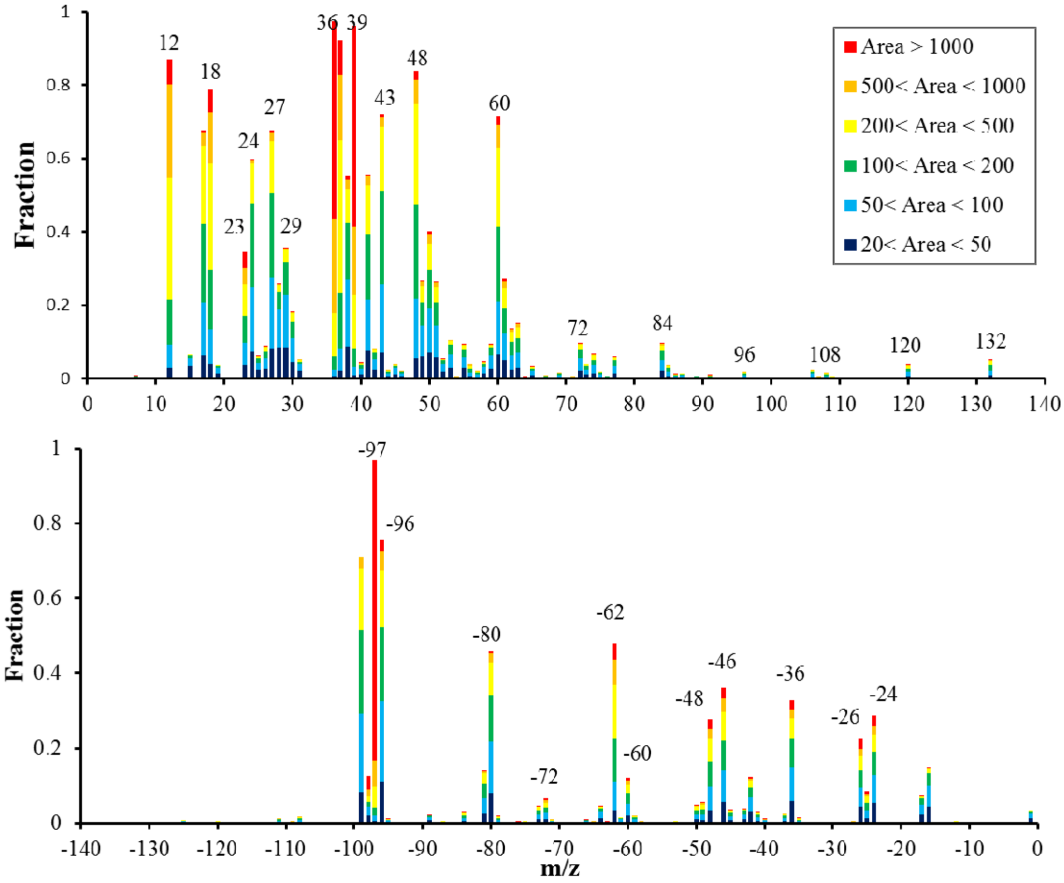

Figure S3. The number-based digitized mass spectrum of cloud-free BC-containing particles at the remote high-altitude site.

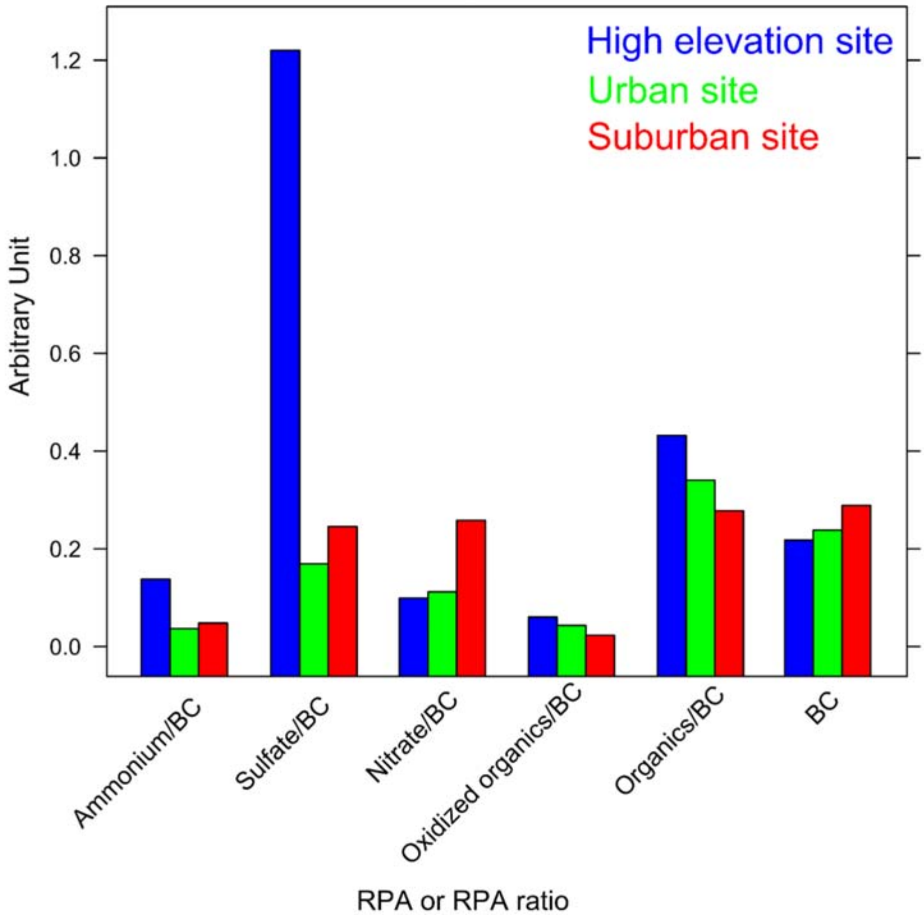

Figure S4. RPA ratio of ammonium (m/z 18), sulfate (m/z -97), nitrate (m/z -62), oxidized organics (m/z 43), and other organics (m/z 27, 50, 51, 61, 63, -26) to BC, and RPA of BC (carbon ion clusters ($C_n^{+/-}$, $n \leq 5$)) at the high elevation site, urban (Guangzhou), and suburban sites (Heshan) during winter in southern China. The particles in Guangzhou and Heshan were similarly measured by SPAMS during winter. Despite of matrix effects due to the laser desorption/ionization for SPAMS, advances have been made in semi-quantifying individual chemical species, either through multivariate analysis or by applying peak intensities for specific ions (e.g., Xing et al., 2011; Jeong et al., 2011; Healy et al., 2013). RPA, defined as the peak area of each m/z divided by the total dual ion mass spectral peak area, is related to the relative amount of a species on a particle. Compared to absolute peak area, RPA was commonly applied because it is less sensitive to the variability in ion intensities associated with particle-laser interactions. It is also noted that matrix effects might be lower when calculation was performed for similar particle type, i.e., BC-containing particles.

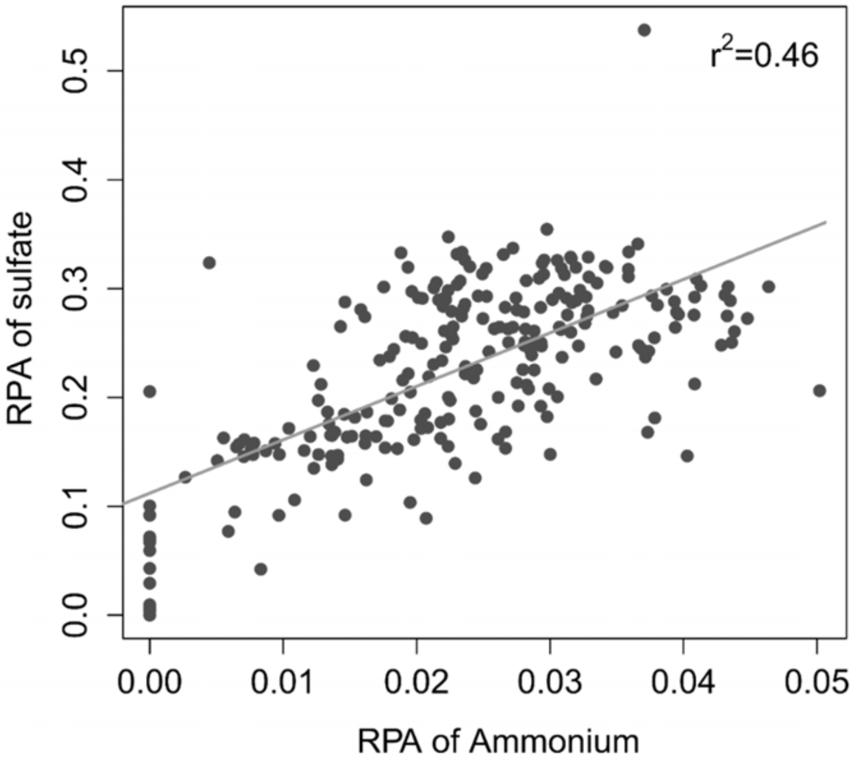

Figure S5. Correlation analysis of hourly average RPA for ammonium and sulfate associated with BC-containing particles. The correlation coefficient is a bit lower than expected might partly due to matrix effect in single particle mass spectrometry (e.g., Xing et al., 2011; Jeong et al., 2011; Healy et al., 2013).

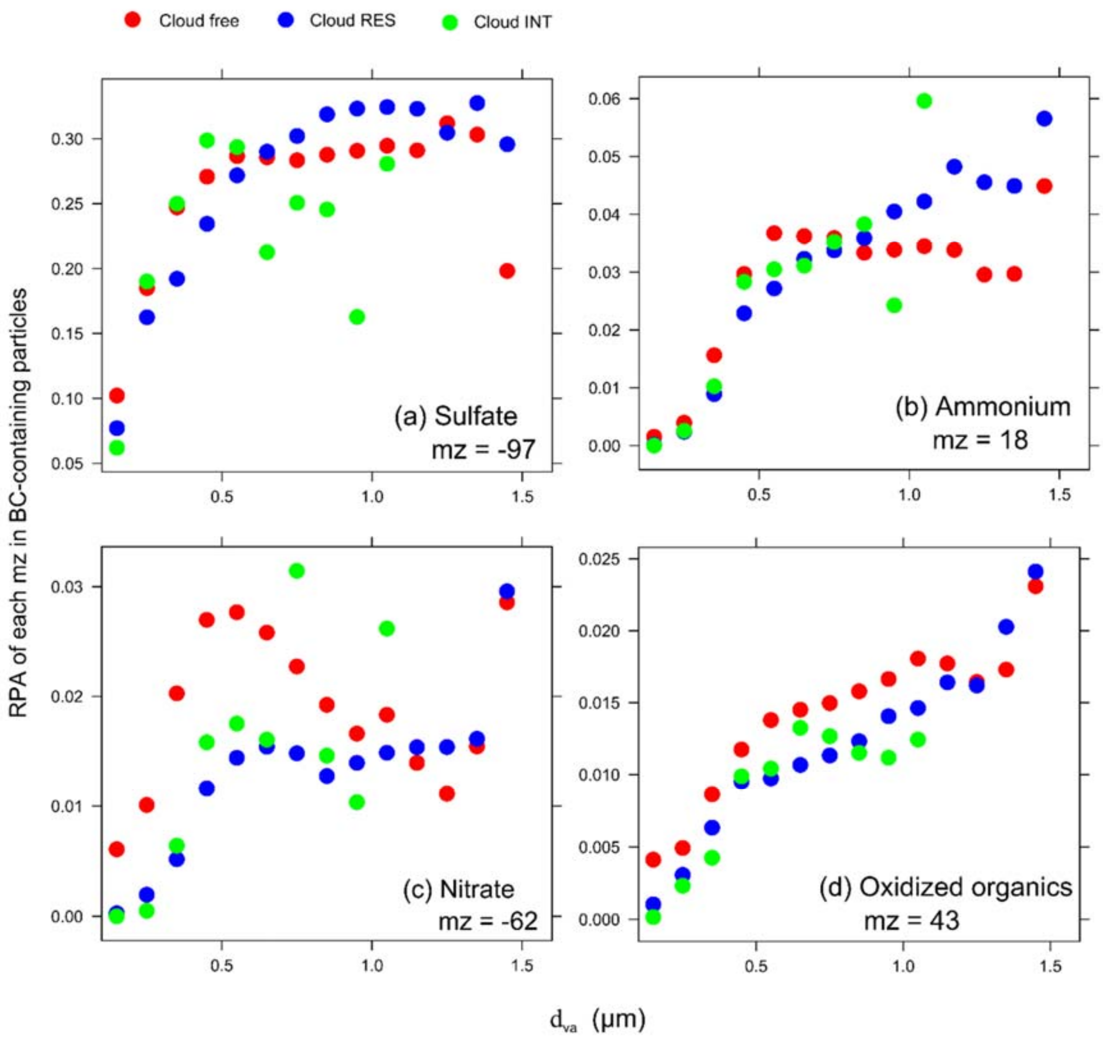

98

99 Figure S6. RPA of each secondary species associated with BC-containing particles in

100 cloud-free, INT, and RES particles as a function of particle sizes.

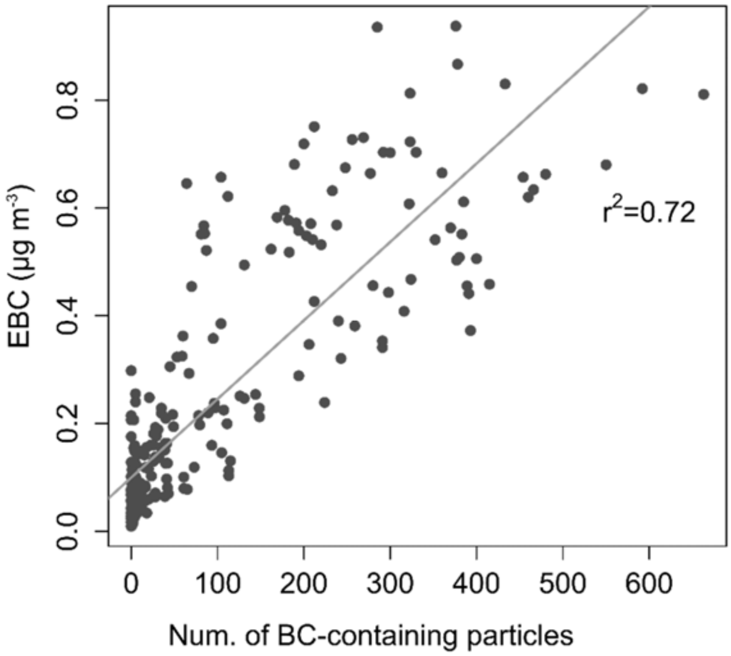

Figure S7. Correlation between time series of Num. of BC-containing particles and concentration of EBC. The volume equivalent diameter of BC particles cores measured in southern China was typically around 200 nm (Huang et al., 2012; Huang et al., 2011). Huang et al. (2011) showed that a large fraction (> 60%) of BC particles are internally mixed with a significant amount of non-refractory materials (coating thickness > 70 nm) at a rural site in southern China. Furthermore, Yu et al. (2010) showed that over 50% of BC are above 500 nm, also indicating internally mixed of BC, with regard that majority of BC particles cores have volume equivalent diameter less than 500 nm (Huang et al., 2012; Huang et al., 2011). As also discussed in section 3.1, BC-containing particles were already heavily mixed with secondary species arriving at our site, and therefore they should be larger enough for the detection by SPAMS.

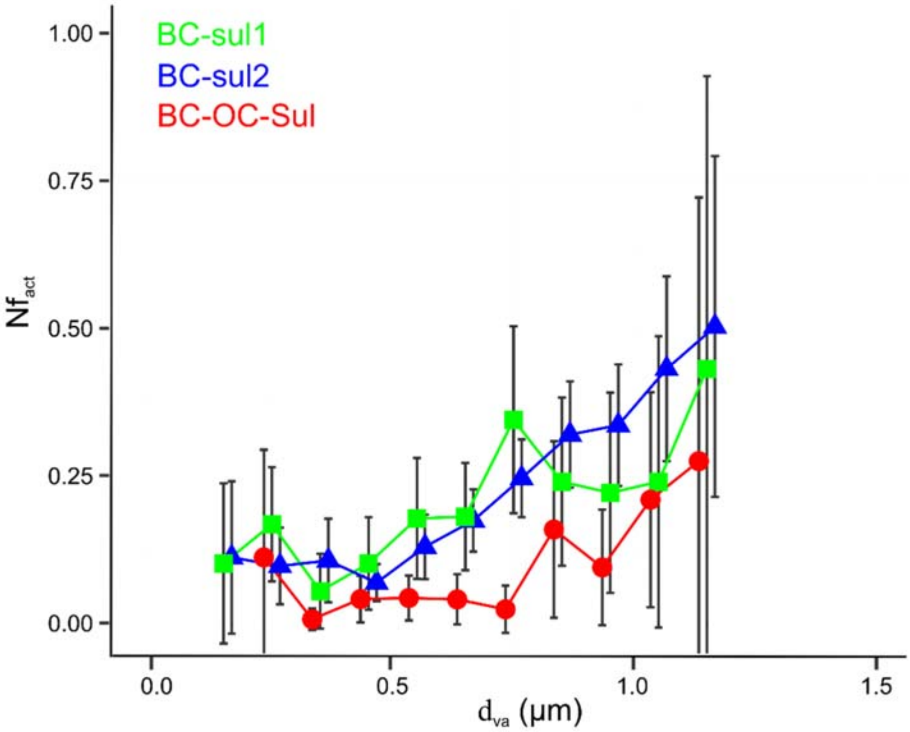

Figure S8. Size-resolved Nf_{act} estimated for three particle types of BC-containing particles. Note that this data only collected during Cloud III event when both cloud RES and INT particles were collected, however, not simultaneously but intermittently. It is noted that although the Nf_{act} for BC-OC-sul type is lower than BC-sul types, the Nf_{act} for all the BC-containing particles is similar to that of all the detected particles. We attributed it to two reasons: (1) BC-OC-sul particles only accounted for ~20% of BC-containing particles, and (2) the other particles also contained OC particles (~10%).

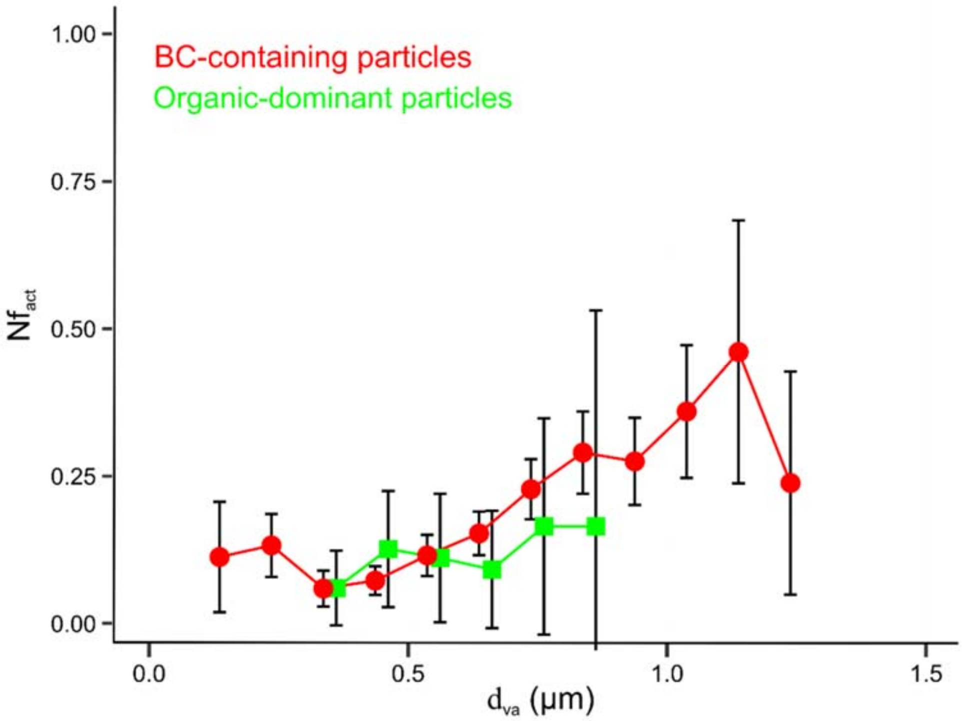

Figure S9. Size-resolved Nf_{act} estimated for BC-containing particles and organic-dominant particles, similar to Fig. S6.

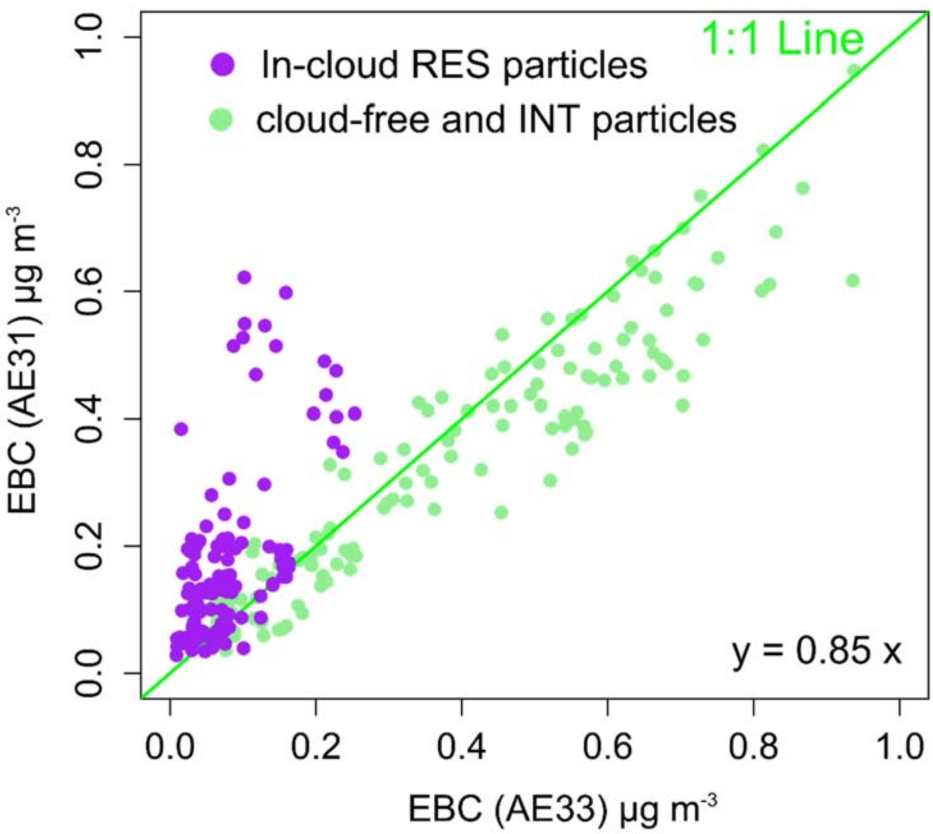

Figure S10. Correlation analysis of EBC measured by AE31 and AE33. They measured the same aerosol for out-of-cloud (including cloud INT and cloud-free) particles. However, during cloud events, AE33 measured cloud RES particles or cloud INT particles for some periods, while AE31 measured cloud INT particles. Therefore, the EBC were compared when the same aerosol were measured, as shown in green dots. The result indicates that they are highly correlated, with EBC measured by AE31 only slightly lower than those by AE33.

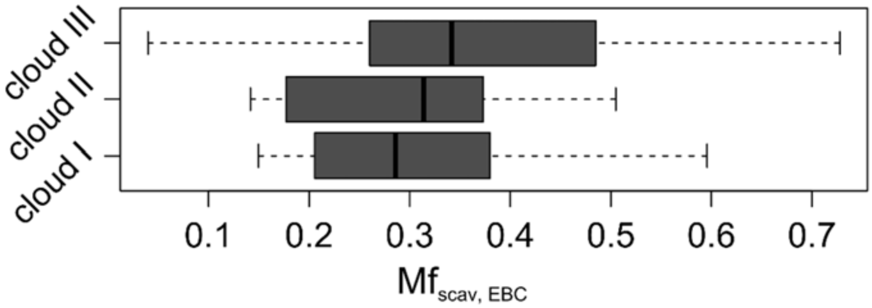

Figure S11. Box and whisker plot of $Mf_{scav,EBC}$ for each cloud event. In a box and whisker plot, the lower, median and upper lines of the box denote the 25th, 50th, and 75th percentiles, respectively, and the lower and upper edges of the whisker denote the 10th and 90th percentiles, respectively.

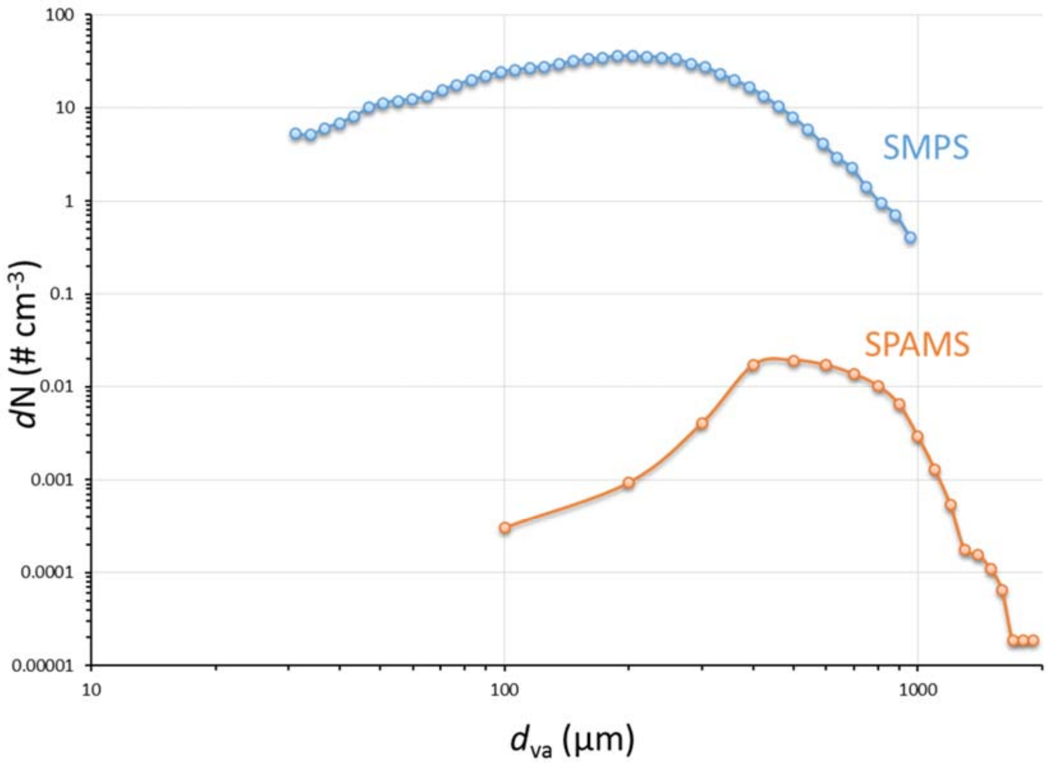

Figure S12. A representative comparison between the size distributions measured by the SPAMS and the SMPS within 12 hours measurements. It should be noted that the diameter is represented as d_{va} by SPAMS, while the diameter measured by the SMPS is represented as electrical mobility diameter (d_m). Herein, the d_m was first converted to the d_{va} for the comparison. The conversion could be simplified to $d_m = d_{va}*\rho_{eff}/\rho_0$ (DeCarlo et al., 2004), where ρ_{eff} refers to the effective density, ρ_0 is the unit density 1.0 g cm^{-3}. The ρ_{eff} is assumed to be 1.5 g cm^{-3} for the calculation (Hu et al., 2012).